Picosecond optically reconfigurable filters exploiting full free spectral range tuning of single ring and Vernier effect resonators

Roman Bruck,[1,*] Ben Mills,[2] David J. Thomson,[2] Benedetto Troia,[3] Vittorio M. N. Passaro,[3] Goran Z. Mashanovich,[2] Graham T. Reed,[2] and Otto L. Muskens[1]

[1] *Physics and Astronomy, Faculty of Physical Sciences and Engineering, University of Southampton, Southampton SO17 1BJ, UK*
[2] *Optoelectronics Research Centre, University of Southampton, Southampton SO17 1BJ, UK*
[3] *Department of Electrical and Information Engineering, Politecnico di Bari, Via E. Orabona 4, 70125 Bari, Italy*
[*]r.bruck@soton.ac.uk

Abstract: We demonstrate that phase shifts larger than 2π can be induced by all-optical tuning in silicon waveguides of a few micrometers in length. By generating high concentrations of free carriers in the silicon employing absorption of ultrashort, ultraviolet laser pulses, the refractive index of silicon can be drastically reduced. As a result, the resonance wavelength of optical resonators can be freely tuned over the full free spectral range. This allows for active integrated optic devices that can be switched with GHz frequencies into any desired state by all-optical means.

References and links

1. K. J. Vahala, "Optical microcavities," Nature **424**, 839-846 (2003).
2. J. Takayesu, M. Hochberg, T. Baehr-Jones, E. Chan, G. Wang, P. Sullivan, Y. Liao, J. Davies, L. Dalton, A. Scherer, and W. Krug, "A hybrid electrooptic microring resonator-based 1x4x1 ROADM for wafer scale optical interconnects," J. of Lightw. Techn. **27**, 440-448 (2009).
3. Q. Xu, B. Schmidt, S. Pradhan, and M. Lipson, "Micrometre-scale silicon electro-optic modulator," Nature **435**, 325-327 (2005).
4. N. Sherwood-Droz, H. Wang, L. Chen, B. G. Lee, A. Biberman, K. Bergman, and M. Lipson, "Optical 4x4 hitless silicon router for optical Networks-on-Chip (NoC)," Opt. Exp. **16**, 15915-15922 (2008).
5. I. Kiyat, A. Aydinli, and N. Dagli, "Low-power thermooptical tuning of SOI resonator switch," IEEE Phot. Tech. Lett. **18**, 364-366 (2006).
6. P. Dong, W. Qian, H. Liang, R. Shafiiha, N. N. Feng, D. Feng, X. Zheng, A. V. Krishnamoorthy, and M. Asghari, "Low power and compact reconfigurable multiplexing devices based on silicon microring resonators," Opt. Exp. **15**, 9852-9858 (2010).
7. A. Martinez, J. Blasco, P. Sanchis, J. V. Galan, J. Garcia-Ruperez, E. Jordana, P. Gautier, Y. Lebour, S. Hernandez, R. Guider, N. Daldosso, B. Garrido, J. M. Fedeli, L. Pavesi, and J. Martí, "Ultrafast all-optical switching in a silicon-nanocrystal-based silicon slot waveguide at telecom wavelengths," Nano Letters **2010**, 1506-1511 (2010).
8. C. Koos, L. Jacome, C. Poulton, J. Leuthold, and W. Freude, "Nonlinear silicon-on-insulator waveguides for all-optical signal processing," Opt. Express 15, 5976-5990 (2007).
9. G. T. Reed, G. Mashanovich, F. Y. Gardes, and D. J. Thomson, "Silicon optical modulators," Nat. Phot. **4**, 518-527 (2010).
10. T. Kampfrath, D. M. Beggs, T. P. White, M. Burresi, D. van Oosten, T. F. Krauss, and L. Kuipers, "Ultrafast rerouting of light via slow modes in a nanophotonic directional coupler," Appl. Phys. Lett. **94**, 241119 (2009).

11. A. Opheij, N. Rotenberg, D. M. Beggs, I. H. Rey, T. F. Krauss, and L. Kuipers "Ultracompact (3 μm) silicon slow-light optical modulator," Sci. Rep. **3**, 3546 (2013).

12. K. Nozaki, T. Tanabe, A. Shinya, S. Matsuo, T. Sato, H. Taniyama, and M. Notomi, "Sub-femtojoule all-optical switching using a photonic-crystal nanocavity," Nat. Phot. **4**, 477-483 (2010).

13. A. C. Turner-Foster, M. A. Foster, J. S. Levy, C. B. Poitras, R. Salem, A. L. Gaeta, and M. Lipson, "Ultrashort free-carrier lifetime in low-loss silicon nanowaveguides," Opt. Exp. **18**, 3582-3591 (2010).

14. S. F. Preble, Q. Xu, B. S. Schmidt, and M. Lipson, "Ultrafast all-optical modulation on a silicon chip," Opt. Lett. **30**, 2891-2893 (2005).

15. Y. H. Wen, O. Kuzucu, M. Fridman, A. L. Gaeta, L. W. Luo, and M. Lipson, "All-optical control of an individual resonance in a silicon microresonator," Phys. Rev. Lett. **108**, 223907 (2012).

16. V. R. Almeida, C. A. Barrios, R. R. Panepucci, and M. Lipson, "All-optical control of light on a silicon chip," Nature **431**, 1081-1084 (2004).

17. T. K. Liang, L. R. Nunes, T. Sakamoto, K. Sasagawa, T. Kawanishi, M. Tsuchiya, G. R. A. Priem, D. Van Thourhout, P. Dumon, R. Baets, and H. K. Tsang, "Ultrafast all-optical switching by cross-absorption modulation in silicon wire waveguides," Optics Express **13**, 7298-7303 (2005).

18. Q. Xu and M. Lipson, "All-optical logic based on silicon micro-ring resonators," Opt. Exp. **15**, 924-929 (2007).

19. T. Tanabe, M. Notomi, S. Mitsugi, A. Shinya, and E. Kuramochi, "All-optical switches on a silicon chip realized using photonic crystal nanocavities," Appl. Phys. Lett. **87**, 151112 (2005).

20. M. Notomi, T. Tanabe, A. Shinya, E. Kuramochi, and H. Taniyama, "On-chip all-optical switching and memory by silicon photonic crystal nanocavities," Advances in Optical Technologies **2008**, 568936 (2008).

21. B. G. Lee, A. Biberman, P. Dong, M. Lipson, and K. Bergman, "All-optical comb switch for multiwavelength message routing in silicon photonic networks," IEEE Phot. Tech. Lett. **20**, 767-769 (2008).

22. P. Dong, S. F. Preble, and M. Lipson, "All-optical compact silicon comb switch," Opt. Exp. **15**, 9600-9615 (2007).

23. M. Waldow, T. Plötzing, M. Gottheil, M. Först, J. Bolten, T. Wahlbrink, and H. Kurz, "25ps all-optical switching in oxygen implanted silicon-on-insulator microring resonator," Opt. Exp. **16**, 7693-7702 (2008).

24. M. Belotti, M. Galli, D. Gerace, L.C. Andreani, G. Guizzetti, A. R. Md Zain, N.P. Johnson, M. Sorel, and R. M. De La Rue, "All-optical switching in silicon-on-insulator photonic wire nano–cavities," Opt. Exp. **18**, 1450-1561 (2010).

25. S. Schönenberger, T. Stöferle, N. Moll, R. F. Mahrt, M. S. Dahlem, T. Wahlbrink, J. Bolten, T. Mollenhauer, H. Kurz, and B. J. Offrein, "Ultrafast all-optical modulator with femtojoule absorbed switching energy in silicon-on-insulator," Opt. Exp. **15**, 22485-22496 (2010).

26. D. K. Tripathi, P. Singh, N.K. Shukla, and H. K. Dixit, "Reconfigurable optical add drop multiplexers A Review," Electrical & Computer Engineering: An International Journal 3, DOI : 10.14810/ecij.2014.3101 (2014).

27. A. V. Tsarev, "Thin heterogeneous optical silicon-on-insulator waveguides and their application in reconégurable optical multiplexers," Quant. El. **38**, 445-451 (2008).

28. P. Prabhathan, Z. Jing, V. M. Murukeshan, Z. Huijuan, and C. Shiyi, "Discrete and fine wavelength tunable thermo-optic WSS for low power consumption C+L band tenability," IEE Phot. Tech. Lett **24**, 152-154 (2012).

29. V. M. N. Passaro, F. Magno, and A. V. Tsarev, "Investigation of thermo-optic effect and multireflector tunable filter/multiplexer in SOI waveguides," Opt. Exp. **13**, 3429-3437 (2005).

30. H. Huang, W. Li, and W. Ren, "Next-generation ROADM architecture and technologies," Adv. Mat. Research **760**, 50-53 (2013).

31. R. Bruck, B. Mills, B. Troia, D. J. Thomson, F. Y. Gardes, G. Z. Mashanovich, V. M. N. Passaro, G. T. Reed, and O. L. Muskens, "Device-level characterization of the flow of light in integrated photonic circuits using ultrafast photomodulation spectroscopy," Nature Photonics **9**, 54–60 (2015).

32. P. Rabiei, W. H. Steier, C. Zhang, and L. R. Dalton, "Polymer Micro-Ring Filters and Modulators," Journ. of Lightw. Techn. **20**, 1968-1975 (2002).

33. B. Troia, A. Z. Khokhar, M. Nedeljkovic, J. S. Penades, V. M. N. Passaro, and G. Z. Mashanovich, "Cascade-coupled racetrack resonators based on the Vernier effect in the mid-infrared," Opt. Exp. **22**, 23990-24003 (2014).

34. T. Claes, W. Bogaerts, and P, Bienstman, "Vernier-cascade label-free biosensor with integrated arrayed waveguide grating for wavelength interrogation with low-cost broadband source," Opt. Lett. **36**, 3320-3322 (2011).

35. T. Claes, W. Bogaerts, and P. Bienstman, "Experimental characterization of a silicon photonic biosensor consisting of two cascaded ring resonators based on the Vernier-effect and introduction of a curve fitting method for an improved detection limit," Opt. Exp. **15**, 22747-22761 (2010).
36. L. Jin, M. Li, and J. J. He, "Optical waveguide double-ring sensor using intensity interrogation with a low-cost broadband source," Opt. Lett. **36**, 1128-1130 (2011).
37. R. Boeck, L. Chrostowski, and N. A. F. Jaeger, "Thermally tunable quadruple Vernier racetrack resonators," Opt. Lett. **38**, 2440-2442 (2013).
38. W. S. Fegadolli, G. Vargas, X. Wang, F. Valini, L. A. M. Barea, J. E. B. Oliveira, N. Frateschi, A. Scherer, V. R. Almeida, and R. R. Panepucci, "Reconfigurable silicon thermo-optical ring resonator switch based on Vernier effect control," Opt. Exp. **20**, 14722-14733 (2012).
39. G. Ren, T. Cao, and S. Chen, "Design and analysis of a cascaded microring resonator-based thermo-optical tunable filter with ultralarge free spectrum range and low power consumption," Opt. Engineering **50**, 074601 (2011).
40. L. Zhou, X. Zhang, L. Lu, and J. Chen, "Tunable Vernier microring optical filters with p-i-p-type microheaters," IEEE Phot. Journal **5**, 6601211 (2013).
41. S. J. Choi, Z. Peng, Q. Yang, S. J. Choi, and P. D. Dapkus, "Tunable narrow linewidth all-buried heterostructure ring resonator filters using Vernier effects," IEEE Phot. Tech. Lett. **17**, 106-108 (2005).
42. K. G. Wilcox, A. H. Quarterman, V. Apostolopoulos, H. E. Beere, I. Farrer, D. A. Ritchie, and A. C. Tropper, "175 GHz, 400-fs-pulse harmonically mode-locked surface emitting semiconductor laser," Opt. Exp. **20**, 7040-7045 (2012).
43. K. G. Wilcox, A. C. Tropper, H. E. Beere, D. A. Ritchie, B. Kunert, B. Heinen, and W. Stolz, "4.35 kW peak power femtosecond pulse modelocked VECSEL for supercontinuum generation," Opt. Exp. **21**, 1599-1605 (2013).
44. R. Boeck, W. Shi, L. Chrostowski, and N. A. F. Jaeger, "FSR-eliminated Vernier racetrack resonators using grating-assisted couplers," IEEE Photon. J. **5**, 2202511 (2013).
45. R. Boeck, J. Flueckiger, L. Chrostowski, and N. A. F. Jaeger, "Experimental performance of DWDM quadruple Vernier racetrack resonators," Opt. Exp. **21**, 9103–9112 (2013).

1. Introduction

Optical resonators are among the most versatile optical elements. Resonances with high quality-factors (Q-factors) are essential for applications in telecommunication, sensing, and nonlinear optics [1]. Silicon-on-insulator (SOI) is an attractive platform to realize integrated optical resonators, as it promises high levels of integration, low loss and compatibility with mass production processes. Among the various types of resonators, ring resonators, or related concepts such as racetrack resonators, are among the best investigated.

By actively tuning the resonance wavelength, tunable wavelength filters, modulators and switches can be created. Mechanisms for resonator tuning have been widely researched and proposed mechanisms include electro-optic tuning [2,3], thermo-optic tuning [4-6], as well as exploiting the Kerr-effect [7,8] and plasma dispersion. Plasma dispersion, i.e. changing the refractive index of silicon by generation of free carriers, can be induced by directly injecting free carriers into the silicon [9], or by absorption of photons with energies above the bandgap in an all-optical way [10,11].

All-optical tuning is desirable as it circumvents the need to transform signals between the optical and the electrical domain. It is believed to eventually be faster and more economical than electronic tuning [12]. SOI based resonators can be all-optically tuned by two-photon absorption of near-infrared light [13-21] or by direct absorption of photons with energies larger than the bandgap, i.e. of wavelengths of typically 800 nm or below [22-25]. Usually, the small change in the refractive index of silicon that can be achieved by all-optical tuning is given as the main drawback. Thus, these pioneering studies often demonstrated all-optical tuning by switching high Q-factor optical resonators between on- and off-states, where large modulations in transmission were achieved within relatively small tuning ranges of the order of the resonance width.
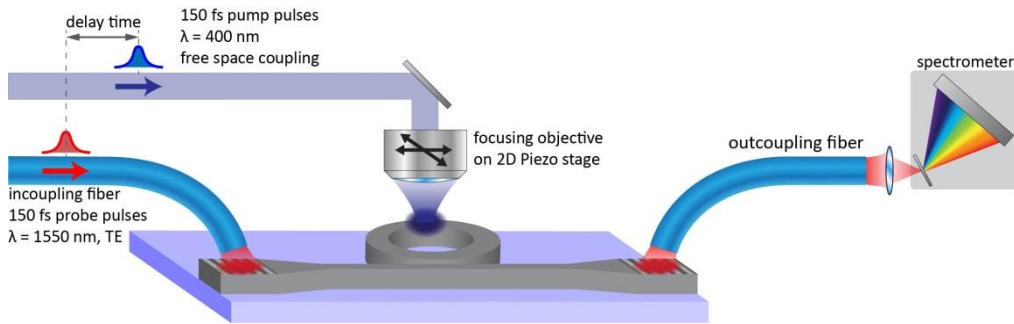
Fig. 1. Optical setup for tuning of optical resonators employing UPMS. Infrared probe pulses are coupled by grating couplers into the input waveguide, travel through the device and are detected after outcoupling in a spectrometer. Pump pulses are focused on the resonator from top.

Here, we demonstrate that all-optically induced phase shifts of more than 2π are possible within conventional SOI waveguides over micrometer lengths by exploiting above-bandgap optical pumping. As a result, resonance wavelengths can be continuously tuned to any desired value within the free spectral range (FSR). We experimentally demonstrate large shifts in the resonance wavelength of a ring resonator as well as for a set of coupled resonators in a Vernier configuration. Picosecond all-optical tuning of resonators opens up new avenues for all-optical devices such as fully tunable wavelength filters and all-optical reconfigurable optical add-drop multiplexers (ROADMs) [26,27]. ROADMs are key elements in wavelength division multiplexed networks and currently rely on wavelength selective switches based on liquid crystal technology, microelectromechanical systems or on thermo-optic actuators [28-30]. Implementing such devices in a compact, integrated, ultrafast and all-optical design would mean a leap in performance in next generation optical networks.

2. Optical setup and method

For the tuning of optical resonators we employed a setup similar to the one previously used for spatio-temporal mapping of optical elements [31]. The ultrafast photomodulation spectroscopy (UPMS) technique exploits optical pumping in the UV range using 400 nm wavelength laser pulses generated by frequency doubling of the 800 nm output from a regenerative amplifier (Coherent RegA). The laser system produces pulses of 150 fs length at repetition rate of 250 kHz. A second output with tunable wavelength in the near infrared was taken from the idler output of an optical parametric amplifier and used to probe the transmission of the device under test.

Figure 1 summarizes the experimental setup. The transverse-electric (TE)-polarized probe pulses were focused into a single mode fiber and were coupled by means of grating couplers into the waveguide. The transmitted light was coupled out of the waveguide by another grating coupler into a single mode fiber and was subsequently coupled into a spectrometer equipped with cooled InGaAs CCD array (Andor Shamrock 500i / iDus). The UV pump light was focused from the top onto the device under test using a 100x, 0.5 N.A. microscope objective (Mitutoyo). The precise position of the pump spot on the device was controlled using a piezo stage, which allowed spatial mapping of the photomodulation response. An optical delay line was used to control the time delay between the pump and probe pulses.

As we have shown in our previous study [31], free carrier concentrations exceeding 10^{20} cm^{-3} can be created by excitation of SOI waveguides with 400 nm laser pulses. As a result, the effective index for the fundamental mode in the waveguide can be decreased by more than 0.4, allowing for phase shifts larger than 2π within a length of a few micrometers.

The smallest achievable pump spot diameter with our setup is smaller than one micrometer. However, to generate large phase shifts, a larger pump spot diameter is desirable

to enlarge the excited section of the waveguide while keeping the pump fluence below the damage threshold of the waveguide. We produced different sizes of the pump spot by defocusing the microscope objective. The resulting pump spot diameter was measured by spatially scanning the objective perpendicular to the waveguide by means of the piezo stage. We define the pump spot diameter as the full width at half maximum of a Gaussian fit to the measured data of the spatial scan. Because the pump spot diameter in our experiments was considerably larger than the waveguide width, we further define the effective pump energy E_{eff} as the energy per pump pulse that incidents the waveguide surface by comparing the illuminated area of the circular pump spot with the illuminated waveguide surface area, i.e. $E_{eff} = E \frac{4*w*d}{\pi d^2}$, where E is the total pump pulse energy as measured before entering the microscope objective, w the waveguide width and d the diameter of the pump spot on the sample surface.

3. Ring resonator

The investigated ring resonator has a diameter of 12 μm and is composed of rib waveguides (450 nm width, 220 nm total thickness, 100 nm slab thickness) with SiO_2 as lower and top cladding. Figure 2(a) shows a micrograph of the ring resonator, with annotations showing the direction of light propagation and position of the pump spot. We introduced the pump pulses from top onto the ring at a position opposite of the bus waveguide, in order to avoid any effects of the optical pumping on the bus waveguide. Figures 2(c)-(f) show scans of the normalized transmission spectra as a function of the pump-probe delay time, for different effective pump energies from 38 pJ to 196 pJ. In conventional pump-probe spectroscopy, a dimensionless ratio of the change in transmission normalized to the transmission itself is usually used to correct for differences in spectral response, drift in the setup, etc. However, in case of large (order unity) changes in the spectral response, this method is not very intuitive and it is often easier to interpret the transmission function itself. A proper normalization of the measured spectra to the Gaussian spectrum of the incident probe pulses in our experiment is complicated, as the transmitted spectrum is affected by the ring resonator. As a result, we exploited a scheme which makes use of the fact that the transfer function of the ring resonator is significantly shifted by the pump laser. In the case of the ring resonator, we estimated the Gaussian spectrum of the probe pulses from a combination of the shifted and unshifted transmission spectra, taking the envelope of maximum intensity and thus correcting the reference spectrum for the dips caused by the ring resonator. Applying this Gaussian reference spectrum for normalization of the measured spectra, the transfer function of the ring resonator can be recovered with high fidelity, as can be seen in Figs. 2(c)-(f). For delay times smaller than -10 ps, the pump pulses arrive at the ring delayed by a time larger than the ringdown time of the probe pulses in the resonator. Thus, the transmitted probe is not influenced by the tuning of the ring resonator as it has already finished its propagation through the ring and the resonance wavelength positions of the ring correspond to the unperturbed situation. At zero delay time, i.e. pump and probe pulses arriving at the same time, a significant shift of the resonance toward shorter wavelengths can be observed. This shift can be attributed to the generation of a free-carrier plasma in the silicon, which has been observed in previous studies [9-11,16,31] to reduce the refractive index of silicon, thus shortening the optical length of the resonator and blue-shifting its resonances. For positive delay times, i.e. pump pulses arriving at the ring earlier than the probe pulses, the plasma effect decays due to the recombination of the free carriers in the time between their generation and the arrival of the probe pulse. In the investigated system, the exponential decay time is of the order of a few hundred picoseconds. If in an application a constant shift of the resonance wavelength is desired, a laser with a higher repetition rate but lower pulse energy could be used to keep free carrier population and thus the wavelength shift within a small window.
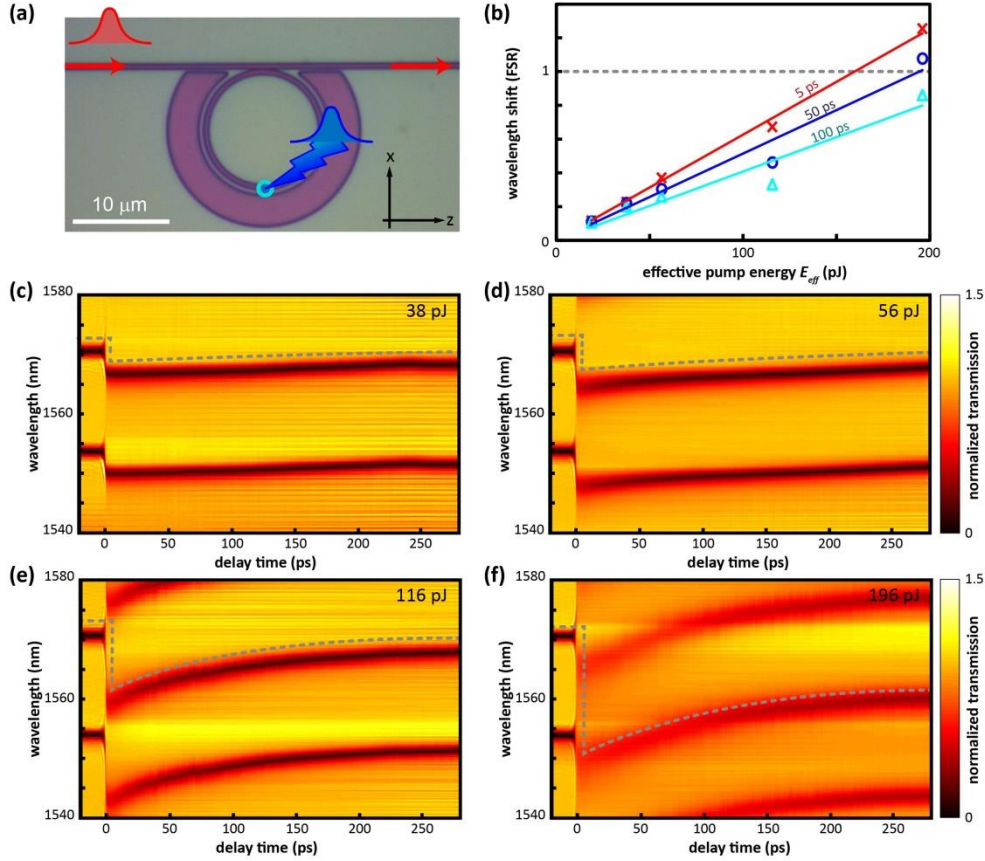
Fig. 2. Tuning of a ring resonator. (a) Micrograph of the investigated ring resonator with indicators for pump position and direction of light propagation. (b) Measured wavelength shift in units of the free spectral range (FSR) for delay times of 5 ps (red crosses), 50 ps (blue circles), and 100 ps (cyan triangles). Solid lines are linear fits to these data points. (c)-(f) Transmission spectra (TE-polarization) of the bus waveguide as a function of delay time at which the ring is modulated for four different effective pump energies. Dips in the transmission spectra (dark colors) correspond to the resonances of the ring and the dashed lines are guides to the eye following the resonances that were used to create (b).

At the longest investigated delay time of 280 ps some blue-shifting of the resonances is still noticeable. Since the thermo-optic coefficient of silicon has a positive sign and would thus redshift resonances, we conclude that this offset is still caused by plasma dispersion and that thermo-optic effects are negligible in our experiments. We extracted the wavelength shift, i.e. the shift of the minima positions in the transmitted spectra, from the measurements presented in Fig. 2(c)-(f) and plotted the wavelength shift (normalized to the FSR of 16.7 nm) versus the effective pump energy in Fig. 2(b) for different delay times. The wavelength shifts follow a linear trend with respect to effective pump energy. For the highest pump energy, we observed tuning of the resonance wavelength by more than 20 nm, thus clearly exceeding the FSR of 16.7 nm. The diameter of the pump spot for this experiment was measured to be 5.8 μm. This demonstrates that within this short length, phase shifts of larger than 2π can be induced by all-optical means.

Figures 3(a)-(c) presents transmission spectra of the bus waveguide for different pump energies and delay times, visualizing the shift of the resonances. Further, the broadening of the resonances due to the absorption induced by the free carriers in the ring resonator becomes apparent. As a result, the quality factor of the resonances is reduced. Figure 3(d) analyses this
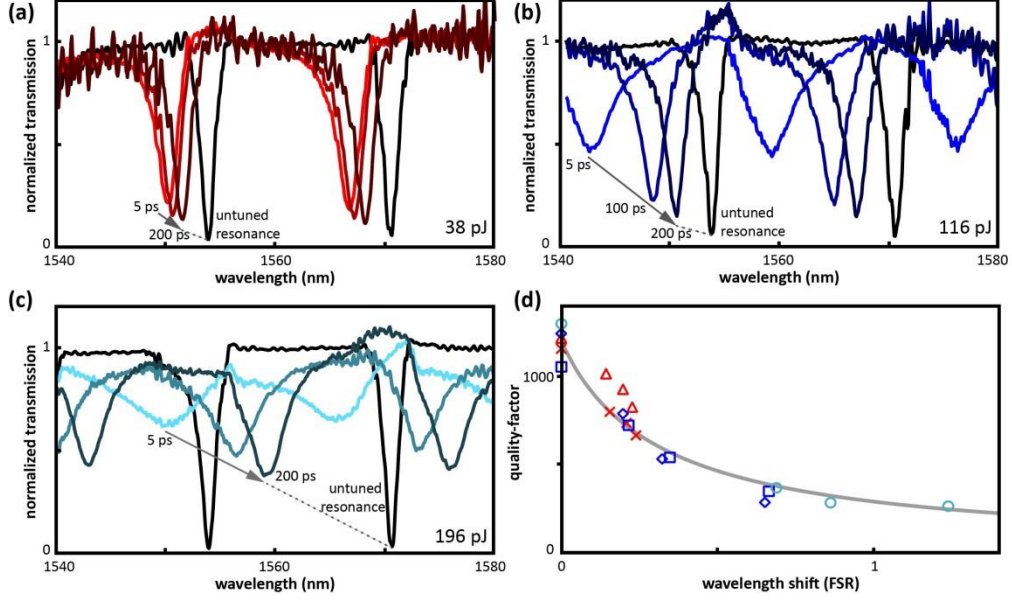
Fig. 3. (a)-(c) Comparison of the untuned spectra of the ring resonator with the spectra for different effective pump energies and for delay times of 5 ps, 100 ps, and 200 ps. (d) Q-factor of the resonances in (a)-(c) versus the wavelength shift normalized to the FSR of 16.7 nm (pump energy 38 pJ: red triangles and crosses, pump energy 116 pJ: blue squares and diamonds, pump energy 196 pJ: cyan circles). The grey line is a fit to the data points assuming a linear relation of $n_i = 0.24 \, \Delta n_r$.

relationship by plotting the quality factor of the resonances in Figs. 3(a)-(c) versus the wavelength shift. The losses due to free carriers in the excited area are reflected in an increase in the imaginary part of the refractive index n_i, while the shift of the resonance wavelengths are caused by a change in the real part of the refractive index Δn_r. Using $Q = \frac{2\pi n_g}{\alpha \lambda}$[32], with the group index determined to be $n_g = 3.72$ from finite element simulations and α the losses in the ring we relate the losses in the ring with the quality factor. We split α into $\alpha = \alpha_u + \alpha_f$, where α_u are the losses in the unmodulated ring and $\alpha_f = k_0 * n_i$ are the additional losses due the exited free carriers. We determine α_u from the average Q-factor of $Q = 1196$ of the unmodulated resonances. By assuming a linear relation between Δn_r and n_i, i.e. $n_i = c * \Delta n_r$, we can optimize the proportional constant c for an optimum fit of the theoretical curve (grey line in Fig. 3(d)) with the measured data points. The calculated constant of $c = 0.24$ is in good agreement with our previous study[31] and is a constant for silicon for this kind of excitation. It inherently links the shift of the resonance wavelength with the reduction of the Q-factor and can only be overcome by using a different material system with a smaller value for c, or a different resonator structure, e.g. Vernier resonators, as discussed below.

In Fig. 4, spatial photomodulation maps for a ring resonator of same nominal dimensions are given. We define the modulation $\Delta T/T$ as the change in transmission ΔT caused by the pump pulses divided by the transmission T of the untuned system. These maps were created by raster-scanning the position of the microscope objective focusing the pump pulses over the area of the ring resonator. Figure 4(a) depicts the spectral position of the maps relative to the tuned and untuned resonances, and sketches the expected photomodulation $\Delta T/T$. The Figs 4(b)-4(f) show the measured photomodulation maps for five different wavelengths around a resonance at 1577 nm. For wavelengths significantly shorter than the original resonance (Figs. 4(b) and 4(c)), the tuning results in a reduction of transmission as the resonance is blue-shifted towards these shorter wavelengths. Transmissions at wavelengths around the original resonance (Figs. 4(d) and (e)) are strongly increased. As expected, the position along the ring
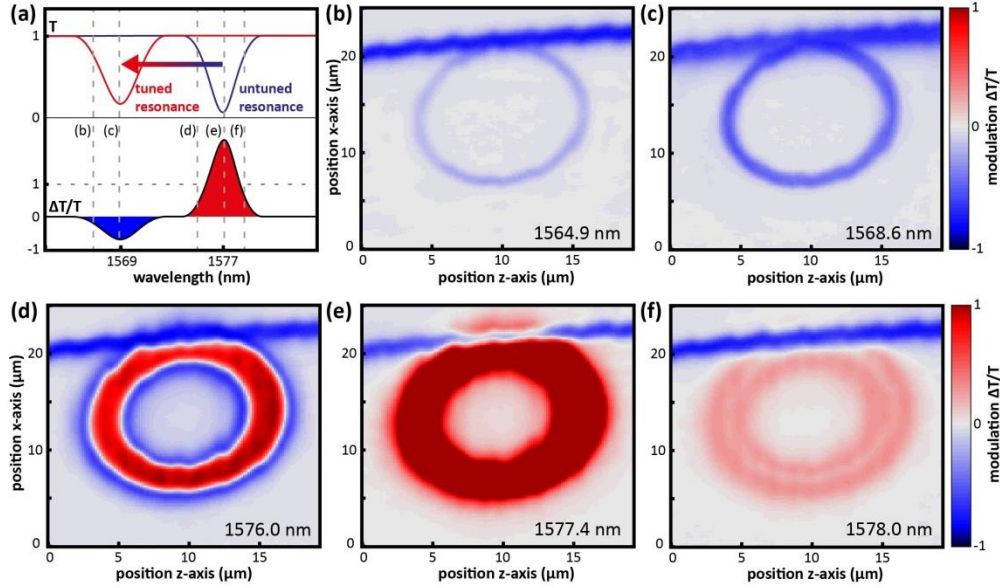
Fig. 4. Spatial photomodulation maps. (a) Sketch of the untuned and tuned transmission spectra *T* of a ring (top curves), as well as of the expected photomodulation Δ*T*/*T* (bottom curve). Also, the spectral positions of the spatial photomodulation maps presented in (b)-(f) are indicated. The spatial maps are plotted for different wavelengths, as denoted in the graphs (3 ps delay time, 95 pJ effective pump energy, 1.5 µm pump spot size).

at which it is modulated has no influence on the strength of the modulation. The blue regions around the main red ring in Fig. 4(d) are caused by a partial overlap of the pump spot with the ring waveguide. In such a scenario, the original resonance wavelength of around 1577.4 nm is blue-shifted towards the investigated wavelength of 1576 nm thus reducing transmission. For better overlap, the resonance wavelength is further driven beyond 1576 nm, leading to the predicted increase in transmission. The bus waveguide is visible as a blue stripe in all five maps. As it is not a resonant structure, the dominant effect on the bus waveguide is absorption caused by the excited free carriers, and thus independent on the wavelength.

4. Vernier resonators

There is a relation between the FSR and the Q-factor that can be achieved using ring resonators. In fact, reducing the ring radius to enlarge the FSR increases bending losses and reduces the Q-factor. However, by coupling resonators, the FSR of the combined system can be a multiple of the FSR of individual resonators. Vernier resonators operating in the second regime are one widely investigated option, e.g. in sensing [33-36]. Towards telecommunication applications, the tuning of Vernier resonators working in the first regime of the Vernier effect has been demonstrated based on the thermo-optic effect [36-40] and by carrier injection [41].

As indicated in Fig. 5(a), we investigate a Vernier system of two racetrack resonators of slightly different lengths coupled by a connecting waveguide and measure the light transmitted through both racetrack resonators. The racetrack resonators and waveguides are composed of SOI rib waveguides (450 nm width, 400 nm total thickness, 180 nm slab thickness) with SiO$_2$ as lower and air as top cladding. The first racetrack has a length of 345.2 µm with a 9.2-µm-long straight coupling region, and the second racetrack is 328 µm long with a 10 µm straight coupling region. Transmission at a given wavelength can only occur if both resonators are in resonance, with the height of the transmission peak defined by the overlap of the transmission peaks of the individual racetracks. Similar to beating
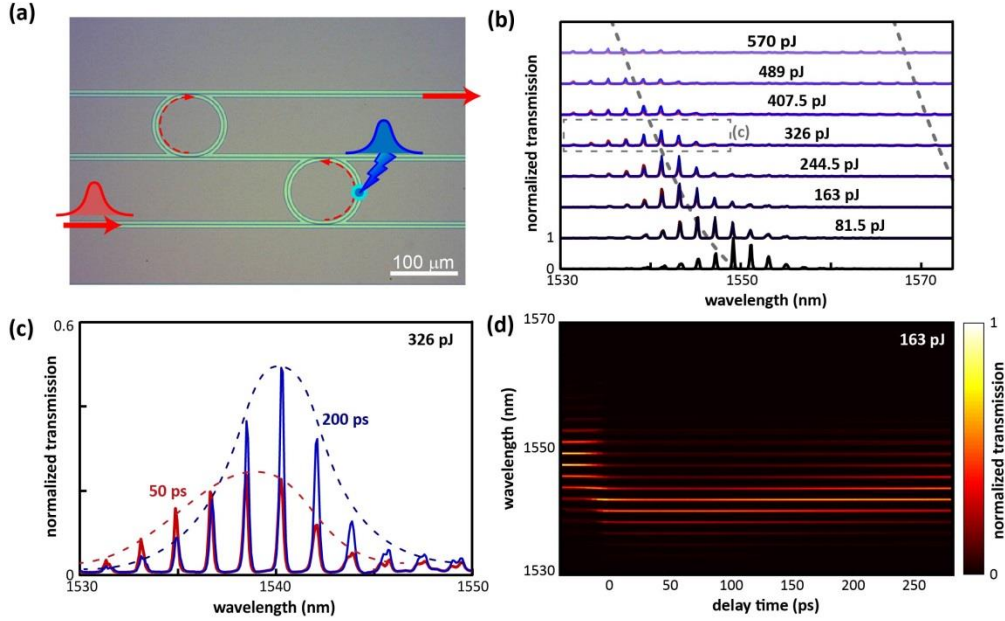
Fig. 5. Tuning of Vernier racetracks. (a) Micrograph of the investigated system with annotations for light propagation and position of the pump spot. (b) Untuned transmission spectrum (black line) and tuned transmission spectra for delay times of 50 ps (red lines) and 200 ps (blue lines) for different effective pump energies. Dashed lines in the background indicate the position of the Vernier envelope maxima. (c) Detailed view on the spectra in (b) for a pump energy of 326 pJ. The dashed lines indicate the envelopes for delay times of 50 ps (red) and 200 ps (blue). (d) Transmission spectra as function of delay time for an effective pump energy of 163 pJ.

phenomena, the transmission peaks are modulated by an envelope defined by the difference in the optical length of the resonators. Tuning the resonance wavelengths of one resonator does not shift the individual transmission peaks, as would be the case for the individual ring resonator. Instead, the envelope is shifted as also occurs in Vernier devices employed for sensing purposes [34,35], where only one of the two cascaded ring resonators is exposed to the analyte to be sensed and undergoes a localized refractive index perturbation. In comparison to a single ring resonator, modulating a Vernier system mitigates negative effects on the Q-factor, as one resonator always remains unaffected. Thus, the Q-factor of the transmitted signal can never fall below the Q-factor of the unmodulated resonator.

In conclusion, an overall Vernier FSR as large as 35.5 nm has been measured experimentally with a Vernier gain of about 20 estimated by means of the first and second racetrack FSRs of 1.76 nm and 1.85 nm, respectively [33].

We investigated the shift of the envelope in Figs. 5(b) and (c). The bottommost curve in Fig. 5(b) shows the untuned transmission spectra. The other curves show tuned spectra with, from bottom to top, increasing pump energy, as denoted in the graph (pump spot diameter 2.8 µm) for delay times of 50 ps (red lines) and 200 ps (blue lines). The presented spectra in Fig. 5 were normalized to the peak transmission of the untuned spectrum. The expected behavior, with the position of the transmission peaks constant, but the envelope shifting, can clearly be seen. For the highest investigated pump energy the envelope shifts by roughly 18 nm, which is one order on magnitude larger than the FSR of the individual racetrack resonators. Further, for higher pump energies, absorption due to the free carriers becomes evident. As the peak positions remain unchanged, the red curves in the background (50 ps) overlap strongly with the blue curves (200 ps). However, by plotting a detailed graph for a pump energy of 326 pJ, Fig. 5(c) reveals that the envelope is more blue-shifted at 50 ps (red

dashed line) than for 200 ps (blue dashed line). Additionally, the overall magnitude of the peaks at 50 ps is smaller and the envelope broader compared to 200 ps. This is consistent as a larger effect on the real and imaginary part of the effective mode index is expected at the shorter delay time. Figure 5 (d) gives an example of transmission spectra as function of delay time for a pump energy of 163 pJ. Expectedly, the time dependence of the plasma dispersion effect in the racetrack resonators is comparable to that of the ring resonator.

5. Conclusion

Optical resonators have been tuned by all-optical pumping employing ultrashort, 400 nm pump pulses. Phase shifts of larger than 2π were demonstrated in waveguide sections shorter than 6 μm, allowing tuning of resonance frequencies over the full free spectral range of the resonator, without dealing damage to the waveguide. The plasma dispersion effect shows an ultrafast rising edge and decays with an exponential time constant of a few hundred picoseconds, allowing for switching speeds in the gigahertz regime.

An important application of our all-optical modulation technique is a novel approach for reconfigurable optical add-drop multiplexing, where resonant wavelengths can be controlled and reconfigured by means of a UV pump signal. Significant progress has been made in the field of compact and affordable fast laser sources with high repetition rates, such as mode-locked vertical-external-cavity surface-emitting-lasers (VECSELs), where compact laser sources with GHz repetition rate, sub-picosecond pulse length and high output power have been reported (e.g. [42,43]). The laser pulse length is not vital to our scheme of all-optical tuning provided it is much shorter than the recombination time of the free carriers. Thus, we believe that by employing these novel laser sources, devices such as ROADMs based on integrated optical circuits and all-optical modulation as presented here will become feasible in the near future and could be realized as low-maintenance devices-in-a-box.

Finally, it is worth specifying that the ultrafast all-optical tuning demonstrated here can be employed in Vernier devices with multiple cascaded ring or racetrack resonators designed to operate in the first regime of the Vernier effect, where FSRs larger than 95 nm [40,44] as well as interstitial peak suppressions up to 40 dB [45] can be achieved for ultra-high performance optical filtering.

Acknowledgments